



1 **Assessment of inter-city transport of particulate matter in the**  
2 **Beijing-Tianjin-Hebei region**

3 Xing Chang<sup>1</sup>, Shuxiao Wang<sup>1,2</sup>, Bin Zhao<sup>3</sup>, Siyi Cai<sup>1</sup>, and Jiming Hao<sup>1,2</sup>

4 [1] State Key Joint Laboratory of Environment Simulation and Pollution Control, School of Environment,

5 Tsinghua University, Beijing 100084, China

6 [2] State Environmental Protection Key Laboratory of Sources and Control of Air Pollution Complex,

7 Beijing 100084, China

8 [3] Joint Institute for Regional Earth System Science and Engineering and Department of Atmospheric and

9 Oceanic Sciences, University of California, Los Angeles, CA 90095, USA

10

11 *Correspondence to:* Shuxiao Wang [shxwang@tsinghua.edu.cn]

12 and Bin Zhao [zhaob1206@ucla.edu]

13



## 14 **Abstract**

15 The regional transport of PM<sub>2.5</sub> plays an important role in the air quality over the Beijing-Tianjin-Hebei (BTH)  
16 region in China. However, previous studies on regional transport of PM<sub>2.5</sub> are mainly at province level, which  
17 is insufficient for the development of an optimal joint PM<sub>2.5</sub> control strategy. In this study, we calculate PM<sub>2.5</sub>  
18 inflows and outflows through the administrative boundaries of three major cities in the BTH region, i.e. Beijing,  
19 Tianjin and Shijiazhuang, using the WRF (Weather Research and Forecasting model) -CMAQ (Community  
20 Multiscale Air Quality) modelling system. The monthly average inflow fluxes indicate the major directions of  
21 PM<sub>2.5</sub> transport. For Beijing, the PM<sub>2.5</sub> inflow fluxes from Zhangjiakou (on the northwest) and Baoding (on  
22 the southwest) constitute 57% of the total in winter, and Langfang (on the southeast) and Baoding constitute  
23 73% in summer. Based on the net PM<sub>2.5</sub> fluxes and their vertical distributions, we find there are three major  
24 transport pathways in the BTH region: the Northwest-Southeast pathway in winter (at all levels below 1000  
25 m), the Southeast-Northwest pathway in summer (at all levels below 1000 m), and the Southwest-Northeast  
26 pathway both in winter and in summer (mainly at 400 – 1000 m). In winter, even if surface wind speeds are  
27 small, the transport at above 400 m could still be strong. Among the three pathways, the Southwest-Northeast  
28 happens along with PM<sub>2.5</sub> concentrations 30% and 55% higher than the monthly average in winter and summer,  
29 respectively. Analysis of two heavy pollution episodes in January and July in Beijing show a much stronger  
30 (8-16 times) transport than the monthly average, emphasizing the joint air pollution control of the cities located  
31 on the transport pathways, especially during heavy pollution episodes.

32

33 Key words: PM<sub>2.5</sub> flux; inter-city transport; CMAQ model; Beijing-Tianjin-Hebei region

34

## 35 **1. Introduction**

36 The Beijing-Tianjin-Hebei (BTH) region, one of the most developed regions in China, is suffering from severe  
37 pollution of particulate matter with diameter less than 2.5 µm (PM<sub>2.5</sub>). According to the monitoring data from  
38 China National Environmental Monitoring Centre (<http://www.cnemc.cn/>), the average PM<sub>2.5</sub> concentrations  
39 of the BTH region in 2013, 2014 and 2015 were 106 µg/m<sup>3</sup>, 93 µg/m<sup>3</sup> and 77 µg/m<sup>3</sup>, respectively, which far  
40 exceeded the 35 µg/m<sup>3</sup> standard of China. The high PM<sub>2.5</sub> concentrations have adverse impacts on visibility  
41 (Zhao et al., 2011b) as well as human health (Zhang et al., 2013), and thus may cause a large economic loss



42 (Mu and Zhang, 2013). Therefore, it is urgent to reduce the  $PM_{2.5}$  pollution in the BTH region.

43 Emissions from one city can substantially affect the  $PM_{2.5}$  pollution in another city under particular  
44 meteorology conditions due to the transport of air pollutants. For example, some studies showed that emissions  
45 from outside Beijing can contribute 28-70% of the ambient  $PM_{2.5}$  concentrations in Beijing (An et al., 2007;  
46 Streets et al., 2007; BJEPPB, 2015; Wang et al., 2014). A number of approaches have been applied to evaluate  
47 the inter-city transport of  $PM_{2.5}$  and its effect on local air quality. The backward trajectory, such as the  
48 HYSPLIT model (Stein et al., 2015), is one of the most commonly used methods. This method can provide  
49 the most probable transport trajectory for the air masses that have arrived at a target location; however, it  
50 cannot quantify the inter-city transport of  $PM_{2.5}$ . Another commonly used method is the sensitivity analysis  
51 based on Euler 3-D models, such as CMAQ (Community Multiscale Air Quality model), which is done by  
52 calculating the change in concentration due to a change in emissions. This method includes the Brute Force  
53 Method (e.g. Wang et al., 2015), the decoupled direct method (DDM, (Itahashi et al., 2012)), and the Response  
54 Surface Model (RSM, (Zhao et al., 2015)). These methods are all based on a chemical transport model, so that  
55 the physical and chemical processes can both be well considered. However, there are gaps between sensitivities  
56 and the contribution of inter-city transport because of the non-linear relationships between emissions and  
57 concentrations (Kwok et al., 2015).

58 Based on the meteorology field and air pollutant concentrations simulated by air quality model, the inter-city  
59 transport of  $PM_{2.5}$  can be easily evaluated by the  $PM_{2.5}$  flux through city boundaries. Compared to the  
60 preceding methods, the flux approach can give direct and quantitative assessment of the transport of pollutants  
61 without a heavy calculation burden. This approach has been widely applied to assess the transport of air  
62 pollutants on a large scale, such as inter-continent transport (Berge and Jakobsen, 1998; In et al., 2007). There  
63 are also studies that evaluated the pollutant transport over a regional scale (Jenner and Abiodun, 2013; Wang  
64 et al., 2009); some of which focused on the BTH region (An et al., 2012; Wang et al., 2010). In those studies,  
65 the boundaries for flux calculations are at the province level. However, in China, the air pollution control  
66 strategy is formulated and implemented at the city level. Moreover, most previous studies regarding  $PM_{2.5}$   
67 transports in the BTH region have focused on Beijing. In recent years, however, under the policy of  
68 “integrating development of BTH region”, the air quality in Tianjin and cities in Hebei Province are being  
69 increasingly emphasized. Therefore, a systematic assessment of the  $PM_{2.5}$  flux at the city level in the BTH  
70 region is needed.



71 In this study, we select Beijing, Tianjin and Shijiazhuang as target cities, and calculate the inter-city PM<sub>2.5</sub>  
72 transport fluxes through the administrative boundaries between the target cities and the neighboring prefecture-  
73 level cities, based on the WRF (Weather Research and Forecasting model) –CMAQ modeling system. Further  
74 the PM<sub>2.5</sub> source for each city and the transport pathway in the BTH region are identified based on the PM<sub>2.5</sub>  
75 transport flux results.

76

## 77 **2. Methodology**

### 78 **2.1. Emission inventory**

79 A multiscale emission inventory is used in this study. For the regions outside China mainland, we use the MIX  
80 emission inventory (Li et al., 2017) for the year 2010. For the China mainland other than the BTH region, we  
81 adopt a gridded emission inventory of 2012 developed in our previous study (Cai et al., 2017). For the BTH  
82 region, we develop a bottom-up emission inventory in 2012. A unit-based approach is used for power plants,  
83 iron and steel plants, and cement plants (Zhao et al., 2008). Emission factor approach is used for other sectors  
84 (Fu et al., 2013; Zhao et al., 2013b). In particular, emissions in Beijing are updated from the bottom-up  
85 inventory developed by Tsinghua University and Beijing Municipal Research Institute of Environmental  
86 Protection (BJEPB, 2010; Zhao et al., 2011a). The emissions of major pollutants by city are shown in Table 1.  
87 Methods for the biogenic emissions, the VOC speciation and the spatial and temporal allocation of emissions  
88 are consistent with our previous studies (Zhao et al., 2013a). The spatial distributions of emissions are shown  
89 in Fig. S1 (see the Supplementary Information (SI)).

90

### 91 **2.2. WRF-CMAQ model configuration**

92 One-way, triple nesting domains are used in WRF-CMAQ model to simulate the meteorology and air pollutant  
93 fields, as shown in Fig. 1. Domain 1 covers mainland China and part of East Asia and Southeast Asia at a grid  
94 resolution of 36 km × 36 km; Domain 2 covers the eastern China at a grid resolution of 12 km × 12 km;  
95 Domain 3 covers the BTH region at a grid resolution of 4 km × 4 km, which is the target area of this study.  
96 The simulation periods are January and July 2012, representing the winter and summer time, respectively.  
97 For the WRF (version 3.7) model, 23 sigma levels are selected for the vertical grid structure with the model  
98 top pressure of 100 mb at approximately 15 km. The National Center for Environmental Prediction (NCEP)'s



99 Final Operational Global Analysis data are used to generate the first guess field with a horizontal resolution of  
100  $1^\circ \times 1^\circ$  at every 6 h. The NCEP's Automated Data Processing (ADP) data are used in the objective analysis  
101 scheme. The major physics options are the Kain-Fritsch cumulus scheme, the Pleim-Xiu land surface model,  
102 the ACM2 planetary boundary layer (PBL) scheme, the Morrison double-moment scheme for cloud  
103 microphysics, and the Rapid Radiative Transfer Model (RRTM) longwave and shortwave radiation scheme.  
104 The Meteorology-Chemistry Interface Processor (MCIP) version 3.3 is applied to process meteorological data  
105 into a format required by CMAQ.

106 We subsequently use CMAQv5.0.2 to simulate the air quality field. The CMAQ model is configured with the  
107 AERO6 aerosol module and the CB-05 gas-phase chemical mechanism. The default profile is used to generate  
108 the boundary condition of the first domain, and the simulation results of the outer domains provide the  
109 boundary conditions for the inner domains. The simulation begins five days ahead to minimize the impact of  
110 initial condition.

111 The model predicted meteorology and  $PM_{2.5}$  concentrations are compared with observation data. The results  
112 are shown in the Supplementary Information (SI). The simulations agree well with observations, with all the  
113 indices within the benchmarks suggested by Emery et al. (2001). We evaluate simulated  $PM_{2.5}$  concentrations  
114 against observations at 5 sites located in Domain 3, i.e., Beijing, Shijiazhuang, Xianghe, Xinglong and  
115 Yucheng (see Fig. 1), as shown in Table 2. The time series of simulated and observed  $PM_{2.5}$  concentrations are  
116 shown in Fig. 2. It can be seen that the variation trends of  $PM_{2.5}$  are well reproduced both in January and in  
117 July for all 5 sites. The average  $PM_{2.5}$  concentrations are slightly underestimated in January, while the  
118 underestimation is larger in July in most sites, especially in Beijing and Xinglong. To understand the reason  
119 of the biases, it is required to evaluate the simulation results of major components of  $PM_{2.5}$ . Given that we  
120 have no observations of  $PM_{2.5}$  components in 2012 in the BTH region, we additionally simulate the air quality  
121 in July and August in 2013, and compare with  $PM_{2.5}$  component observations at several sites (see details in the  
122 SI). Generally, the underestimation of total  $PM_{2.5}$  in the summer time mainly comes from the underestimation  
123 of organic carbon (OC) and sulfate. The default CMAQ tends to underestimate secondary organic aerosol to a  
124 large extent, especially in summer when photochemical reactions are active, which is a common problem of  
125 most widely used chemical transport models (Simon and Bhawe, 2012; Heald et al., 2005; Zhao et al., 2016).  
126 The lack of aqueous oxidation of  $SO_2$  by  $NO_2$  (Wang et al., 2016), and  $SO_2$  oxidation at dust surface (Fu et al.,  
127 2016) may partly account for the underestimation in sulfate. The underestimation in sulfate also partly explains



128 the overestimation in nitrate. In conclusion, the biases of simulated meteorological field and PM<sub>2.5</sub>  
129 concentrations fall in a reasonable range. The modelling results can be used for further studies.

130

### 131 **2.3. PM<sub>2.5</sub> flux calculation**

132 The PM<sub>2.5</sub> flux in this study stands for the mass of PM<sub>2.5</sub> flowing through a particular vertical surface in a  
133 particular period of time. The vertical surface extends from the ground to a particular vertical level along the  
134 boundary of two regions (Fig. 3(a)). However, the models can only provide a three-dimensional discrete wind  
135 field and PM<sub>2.5</sub> concentration field. Therefore, the vertical surface through which the flux is calculated is  
136 discretized to several vertical grid cells, as is illustrated in Fig. 3(b) and detailed in the next paragraph. In this  
137 case, the expression of PM<sub>2.5</sub> flux can be written as

$$138 \quad Flux = \sum_{i=1}^h \sum_l LH_i c \vec{v} \cdot \vec{n} \quad (1)$$

139 where  $l$  is the boundary line;  $h$  is the top layer;  $L$  is the grid width;  $H_i$  is the height between layer  $i$  and  $i-1$ ;  $c$   
140 is the concentration of PM<sub>2.5</sub> on the vertical grid cell;  $\vec{v}$  is the wind vector, and  $\vec{n}$  is the normal vector of the  
141 vertical grid cell. The variables in the expression can be obtained from the output of the models. We choose  
142 the 9<sup>th</sup> layer (about 1000 m) from the ground as the top layer in flux calculation, because most of the PM<sub>2.5</sub>  
143 transport between regions happens inside the boundary layer (Shi et al., 2008). Even though the transport could  
144 happen above the boundary layer, the influence of such transport on the near ground concentrations are less  
145 important because of weaker vertical mixing above the boundary layer.

146 Beijing and Tianjin are two most important and developed megacities in the BTH region. Shijiazhuang is the  
147 capital city, and also one of the most developed and polluted cities in Hebei province. Therefore, we choose  
148 these three cities as the target cities for flux calculation. In order to accurately distinguish the transport from  
149 different adjacent cities and to understand the net PM<sub>2.5</sub> inflow of a city as a whole, all the administrative  
150 boundaries between the target city and the adjacent cities are chosen as the boundary line. The boundary lines  
151 are separated to different segments by neighbor cities, and the fluxes are calculated separately for each segment  
152 of the boundary. The locations of the three target cities and their neighbors are shown in Fig. 1. Note that  
153 because there is a small area which is surrounded by Beijing and Tianjin but belongs to the city of Langfang,  
154 the boundaries between Beijing and Tianjin, Beijing and Langfang, and Tianjin and Langfang are all separated  
155 into two segments. To distinguish them, we add the relative location of the boundary to the neighbor city's



156 name, like “Beijing (N)” and “Beijing (S)”.

157 The flux through a boundary varies every now and then, depending on the wind direction. The polluted air  
158 mass may flow in, affect the local air quality and flow out subsequently in a short time, so that the flux may  
159 offset each other during the integration. Therefore, to characterize the intensity of interactions between two  
160 regions as well as the general impact of PM<sub>2.5</sub> transport, three indices are chosen in regard to the flux  
161 calculation, that is the inflow flux, outflow flux and net flux.

162

### 163 **3. Results and discussion**

#### 164 **3.1. Characteristics of the inter-city PM<sub>2.5</sub> transport in January**

165 The monthly inflow, outflow and net fluxes through each boundary segment of the three target cities are shown  
166 in Fig. 4, from which we can get an overview of the transport in a relatively long period of time. We treat the  
167 fluxes as positive if PM<sub>2.5</sub> flows into the target cities, and vice versa. Therefore, the positive total net fluxes in  
168 Beijing and Shijiazhuang reveal that the PM<sub>2.5</sub> flows into these two cities generally exceed the flows out, and  
169 that these cities act as a “sink” of PM<sub>2.5</sub>. This is possibly due to the unique terrain of Beijing and Shijiazhuang.  
170 These two cities are both half-surrounded by western and northern mountains, while major emissions of PM<sub>2.5</sub>  
171 lie to the south and east. Consequently, pollutants are easily trapped in the bulging part of the plain if there is  
172 a weak wind from the south or the east. The trapped pollutants are either scavenged by wet deposition without  
173 flowing out, or diluted by strong vertical convection due to the strong northwestern wind brought by the cold  
174 front and thus flow out of the boundary layer. In contrast, Tianjin behaves as a “source” of PM<sub>2.5</sub> flux.  
175 Furthermore, a probe into the detailed inflow, outflow and net fluxes through each boundary segment of the  
176 three cities may help to understand to what extent the cities interact with their neighbors. For Beijing, in winter,  
177 the inflow fluxes mainly come from Zhangjiakou (on the northwest) and Baoding (on the southwest), and the  
178 outflows go to Chengde (on the northeast) and Langfang (on the southeast) more than others. For Tianjin,  
179 Langfang (on the northwest) and Tangshan (on the northeast) contribute most of the inflow fluxes, and the  
180 Bohai sea (on the southeast) and Tangshan again receive the major outflow fluxes. Shijiazhuang acts  
181 differently from Beijing and Tianjin. The inflow and outflow fluxes through all the four boundary segments  
182 are considerably strong, with Xingtai (on the south) and Baoding (on the northeast) contributing relatively  
183 more to inflow and outflow fluxes, respectively.



184  $PM_{2.5}$  fluxes may vary with height. We calculate the vertical distribution of net flux through each boundary  
185 segment to see at what level the transport mainly occurs. The results are shown in Fig. 5 (a), (c) and (e). The  
186 fluxes are shown for each vertical layer of the CMAQ model, with the approximate elevation marked to the  
187 left. Generally, the total flowing intensity is stronger at higher levels for all three cities, while the major  
188 contributor varies with layer. If we add up the net fluxes through all boundary segments (shown by the narrow  
189 bars with an envelope line), we can see that the “sink” behavior of Beijing is mainly contributed by the total  
190 net fluxes at 400 to 600 m where contribution from Baoding (on the southwest) exhibits a rapid increase with  
191 height. Similarly, total net flux for Tianjin peaks near 600 m where Tangshan (on the northeast) receives much  
192 more outflow than it does near the ground. Total net flux for Shijiazhuang peaks near 400 m where Hengshui  
193 (on the east) and Xingtai (on the south) make dominant contributions.

194 In order to better understand the general image of the transport characteristics in the BTH region, we use  
195 arrows to represent the net transport fluxes on a map. The result of January is shown in Fig. 6(a). The size of  
196 the arrows represents the amount of the fluxes, while white and black arrows denote fluxes at the lower (layer  
197 1-4 in the model, from the ground to about 400 m) and upper (layer 5-9 in the model, from about 400 m to  
198 about 1000 m) layers, respectively. From the map we can identify two key  $PM_{2.5}$  transport pathways in the  
199 BTH region in January: the Northwest-Southeast pathway (Zhangjiakou -> Beijing -> Langfang -> Tianjin ->  
200 The Bohai Sea) and the Southwest-Northeast pathway (Xingtai -> Shijiazhuang -> Baoding -> Beijing ->  
201 Chengde). The former one is related to the prevailing wind direction brought by winter monsoon in the BTH  
202 region, and happens at both lower layers and higher layers. The latter one happens mainly at higher layers.

203 According to the Ekman Spiral, wind speed is much higher at the upper level of the boundary layer (Holton  
204 and Hakim, 2012), so that pollutants can travel a longer distance during their lifetime. Assuming that the  
205 emission height of each city is similar, we believe that the higher altitude  $PM_{2.5}$  flows in, the farther the source  
206 it comes from. From this point of view, the  $PM_{2.5}$  flow of the Southwest-Northeast pathway at higher levels  
207 may consist of a relatively long range transport. In winter time, the southwest wind field usually occurs after  
208 the passage of a cold high pressure, when the wind speed is low and the sky is clear. Such air condition traps  
209 less upward infrared radiation at night, which helps to enhance the air stability, or even causes temperature  
210 inversion. Moreover, the southwest wind also brings moisture, leading to the formation of fog, which may  
211 enhance the aqueous reaction to form more particles. Therefore, southwest wind is usually accompanied by  
212 pollution. The Southwest-Northeast transport pathway should be intensely considered in the winter time of the





213 BTH region. In contrast, the northwest wind usually comes during the passage of a cold high pressure, with  
214 relatively high wind speed both at lower and higher levels, bringing dry, cold and clean air from the non-  
215 polluted area. The large fluxes from northwest are more likely due to the strong winds rather than the high  
216  $PM_{2.5}$  levels.

### 217 3.2. Characteristics of the inter-city $PM_{2.5}$ transport in July

218 We conduct the same calculation in July to probe into the transport characteristics in summer. The monthly  
219 average inflow, outflow and net fluxes are shown in Fig. 4. Similar to January, total net fluxes are positive  
220 (more inflow than outflow) for Beijing and Shijiazhuang, and negative (more outflow than inflow) for Tianjin,  
221 though the magnitude is much higher than that in January. In detail, the inflow fluxes of Beijing mainly come  
222 from Langfang (on the southeast) and Baoding (on the southwest), and the outflow fluxes are mainly to  
223 Chengde (on the northeast) and Zhangjiakou (on the northwest). For Tianjin, Bohai sea (on the east) and  
224 Tangshan (on the northeast) contribute a large part of inflow, and Langfang (on the northwest) and Tangshan  
225 receive most of the outflow fluxes. The transport directions for Beijing and Tianjin in July are quite different  
226 from those in January. However, for Shijiazhuang, all of the four directions (Shanxi, Baoding, Hengshui and  
227 Xingtai) still contribute comparable amount of inflow and outflow fluxes, with slightly larger inflows from  
228 Xingtai (on the south) and Hengshui (on the east).

229 Fig. 5 (b), (d) and (f) display the vertical distributions of monthly average net fluxes with respect to the three  
230 cities in July. For Beijing, the total net fluxes are positive at all levels, which are different from those in January.  
231 The major contributor Baoding and Langfang show different behaviors. Net flux from Baoding is nearly zero  
232 near the ground, but increases rapidly with height, while the net flux from Langfang (including both Langfang  
233 (N) and Langfang (S)) is significant at all levels, and is largest at medium height. These phenomena are tied  
234 to the wind speed and direction at different heights in the BTH region in summer. The dominant wind direction  
235 near ground is from southeast. Within the boundary layer, the wind will rotate clockwise and become stronger  
236 with height, according to Ekman Spiral (Holton and Hakim, 2012). Langfang and Baoding are located to the  
237 southeast and southwest of Beijing, respectively. The increase of wind speed and the rotation of wind direction  
238 will constantly enhance the  $PM_{2.5}$  transport from southwest, but could contribute oppositely to the transport  
239 from southeast, causing a local maximum in middle layers. For Tianjin, the overall outflow happens mainly at  
240 levels below 600 m, where the outflow flux mainly goes to Langfang. The inflow flux is dominated by the



241 Bohai Sea at all heights, indicating a cross-sea transport from Shandong or other areas. The vertical distribution  
242 of net fluxes for Shijiazhuang is quite similar to that in January, except that Shanxi does not contribute a  
243 considerable amount of inflow flux any more.

244 We also show the general transport characteristics in the BTH region with arrows on the map, as is shown in  
245 Fig. 6(b). Compared with that in winter, the transport at lower layers becomes stronger. We can also figure out  
246 two major transport pathways in BTH in July: the Southwest-Northeast pathway (Xingtai -> Shijiazhuang ->  
247 Baoding -> Beijing -> Chengde), and the Southeast-Northwest pathway (Bohai -> Tianjin -> Langfang ->  
248 Beijing -> Zhangjiakou, and Hengshui -> Shijiazhuang). The latter pathway, which is caused by the summer  
249 monsoon, is significant at both lower and upper layers. The pathway from southwest to northeast is only  
250 obvious at upper layers. Note that in summer the vertical mixing is stronger. Therefore, although the  
251 Southwest-Northeast pathway is only active at higher levels, the transport may still affect the near-ground  
252 concentration remarkably.

253 If we put together the transport characteristics in winter and summer, we can see that, aside from the opposite  
254 transport pathways brought by the monsoon in different seasons, there is a steady transport pathway from  
255 southwest to northeast in the BTH region regardless of the season. This pathway has also been found in some  
256 other studies. Wu et al. (2017) analyzed the regional persistent haze events in the BTH region during 1980-  
257 2013, and found that southwestern wind field at 925 hPa (~800 m) is a typical meteorology condition.  
258 Backward trajectory studies by Zhao et al. (2017) also found a southerly transport pathway during pollution  
259 periods in the BTH region. Therefore, the Southwest-Northeast pathway is indeed important in the BTH region.  
260 The monthly transport characteristics could bring us inspiration on how the joint control of different cities  
261 should be applied. The transport pathway that happens at lower layers suggests that we should primarily  
262 control nearby low-level emission sources, while the pathway at upper layers calls for the control over a larger  
263 region to the upstream direction.

264

### 265 3.3. Characteristics of PM<sub>2.5</sub> transport during heavy-pollution episodes

266 Here we present the net PM<sub>2.5</sub> fluxes of Beijing during two heavy-pollution episodes in January and July of  
267 2012 as examples. In January, we choose 17<sup>th</sup> and 18<sup>th</sup>, which are the two most polluted days (the simulated  
268 PM<sub>2.5</sub> daily average concentrations 211 µg/m<sup>3</sup> and 271 µg/m<sup>3</sup>) throughout the month. In July, we also choose



269 the period with the highest concentration, i.e. 18<sup>th</sup> to 20<sup>th</sup>. The results are shown in Fig. 7 (a-b).

270 The magnitude of net fluxes in the two days in January (-14 kt/day and 17 kt/day) is much higher than the  
271 monthly average value. For 17<sup>th</sup> Jan, there are some weak outflows mainly to Langfang at lower levels, while  
272 stronger inflows from Baoding and Zhangjiakou occur at 300-600m. On 18<sup>th</sup> Jan, fluxes at lower level remain  
273 relatively small though the inflow and outflow directions reverse. However, strong inputs from Baoding and  
274 Langfang at above 400m become significantly strong. It can be seen that although the fluxes near the ground  
275 are small, the inflow transport can be quite strong at levels above 300 m. Coincidentally, the elevation of the  
276 mountains in the northwest of Beijing are commonly higher than 300 m, making it harder for the inflowing  
277 PM<sub>2.5</sub> to flow out. The large amount of PM<sub>2.5</sub> inflows can only be efficiently blown out to the northeast  
278 direction (Chengde, Langfang (N) and Tianjin (N)). These results are consistent with Jiang et al. (2015), who  
279 also found a strong southerly input at a high level during a haze episode in winter. Therefore, the Southwest-  
280 Northeast pathway is of great importance during this heavy pollution period.

281 For the day with the highest concentration in July (July 20<sup>th</sup>), the vertical distribution does not show much  
282 difference from the average of July (Fig. 5 (b)), except for the magnitude. The fluxes are about 1/5 of the  
283 monthly average, or less than 1/10 of that in the heavy-pollution period in January. This result suggests that  
284 the heavy pollution in Beijing in 20<sup>th</sup> July is not dominated by the inter-city transport during that very day.  
285 However, situations are totally different on 18<sup>th</sup> July (Fig. 7 (c)), the first day when the simulated PM<sub>2.5</sub>  
286 concentration reaches a high level in this pollution episode. The magnitude of fluxes is about 6 times larger  
287 than the monthly average, or some 30 times larger than that on 20<sup>th</sup> July. More importantly, the outflow flux  
288 is much smaller than the inflow flux contributed mainly by Baoding and Langfang, which correspond to the  
289 Southwest-Northeast and Southeast-Northwest pathways respectively. Therefore, we can draw an image about  
290 how the PM<sub>2.5</sub> transport affects the air quality in Beijing during this pollution episode. On 18<sup>th</sup> July, the PM<sub>2.5</sub>  
291 start to flow into Beijing through the Southeast-Northwest and Southwest-Northeast pathways with a very  
292 strong flux, but very few of them flow out, causing the accumulative increase of PM<sub>2.5</sub> concentration. On 20<sup>th</sup>  
293 July, the wind field become stable and the transport weakened, but the PM<sub>2.5</sub> that have flowed in before  
294 accumulate to form the heavy pollution. This result indicates that both the Southeast-Northwest and the  
295 Southwest-Northeast pathway are important for Beijing during this polluted period, and the emission from  
296 outside Beijing should be controlled at least 2 days in advance to reduce the peak concentration.

297 From the discussions above, we can see that PM<sub>2.5</sub> transport plays an important role in the heavy-pollution



298 periods in Beijing. We further analyze the PM<sub>2.5</sub> flux data of the three cities day by day, and try to identify the  
299 presence of transport pathway for each day in Beijing, based on whether the inflow flux from a certain direction  
300 is significantly larger than the others. Finally, 8 days in January and 4 days in July are subject to the transport  
301 of Southwest-Northeast pathway, 22 days in January are subject to the transport of Northwest-Southeast  
302 pathway, and 8 days in July are subject to the transport of the Southeast-Northwest pathway. In July, there are  
303 other 8 days subject to both the Southeast-Northwest pathway and the Southwest-Northeast pathway (“SE-  
304 NW + SW-NE” for short). Moreover, some days do not show a clear transport direction, which are referred to  
305 as “unclassifiable days”. We calculate the average simulated concentration for each transport pathway. The  
306 results are shown in Table 3.

307 The days with Southwest-Northeast pathway shows the highest PM<sub>2.5</sub> average concentrations among all days  
308 in both January and July. Therefore, the Southwest-Northeast pathway should be the focus of control strategies.  
309 In contrast, the Northwest-Southeast pathway tends to happen along with the lowest concentrations in both  
310 seasons. Note that in January, the day with the highest concentration (January 19<sup>th</sup>) is coincidentally identified  
311 as the Northwest-Southeast pathway. That day is on the eve of the rapid clearing by the northwest wind (Fig.  
312 2(a)). While the cold front is passing, the heavy polluted air mass is forced to move from northwest to southeast,  
313 which cause a significant transport. However, since the pollution brought by such transport usually happen  
314 with a strong cold front, the PM<sub>2.5</sub> concentration will soon become very low (Jia et al., 2008). If we exclude  
315 January 19<sup>th</sup> from the Northwest-Southeast pathway days, the average concentration will be only 48.5 µg/m<sup>3</sup>.  
316 In July, the Southeast-Northwest pathway and the Southwest-Northeast pathway happen simultaneously for 8  
317 days. The average concentration is 47.4 µg/m<sup>3</sup>, the second highest in July, which further emphasizes the  
318 importance of the transport from the southwest. In summary, the Southwest-Northeast pathway should be taken  
319 great consideration both in January and July, followed by the Southeast-Northwest pathway in July.

320

#### 321 4. Conclusions

322 By calculating PM<sub>2.5</sub> inflow and outflow fluxes through the boundaries between each two prefecture-level  
323 cities, this study has shown the major PM<sub>2.5</sub> input and output directions in winter and summer for Beijing,  
324 Tianjin, and Shijiazhuang. For Beijing, the inflow fluxes mainly come from northwest and southwest in winter,  
325 and southeast and southwest in summer. For Tianjin, the inflow fluxes are mostly from northwest and northeast



326 in winter, and east and northeast in summer. In Shijiazhuang, however, the four neighboring regions contribute  
327 comparable amount of inflow fluxes both in winter and summer.

328 By analyzing the net  $PM_{2.5}$  fluxes and their vertical distribution, we identify several major transport pathways  
329 and the height they occur: the Northwest-Southeast pathway in winter (at all levels below 1000 m, but stronger  
330 at levels above 400 m), the Southeast-Northwest pathway in summer (at all levels below 1000 m), and the  
331 Southwest-Northeast pathway both in winter and in summer (at levels between 400 m and 1000 m). Although  
332 the third pathway does not happen as frequently as the other two in corresponding seasons, it is accompanied  
333 by quite high  $PM_{2.5}$  concentrations in both seasons. Additionally, the relatively large transport height of this  
334 pathway suggests the importance of the long-range transport of  $PM_{2.5}$  on air quality. Specially, in winter, even  
335 if the wind speed near the ground is low, which we often refer to as “steady” conditions, the transport above  
336 400 m, which is primarily associated with long-range transport, could still be strong. These findings suggest  
337 that the joint control for cities on the Southwest-Northeast pathway should be emphasized both in winter and  
338 summer.

339 We also find that inter-city transport during heavy-pollution episodes could be stronger than the monthly  
340 average, at least for the two polluted periods investigated in this study. In the heavy pollution episode in  
341 summer,  $PM_{2.5}$  flows into Beijing and accumulates for two days, leading to a heavy pollution. Therefore,  
342 mitigating emissions from a larger area may be essential for the control of ambient  $PM_{2.5}$  in Beijing. Moreover,  
343 it appears important to control the upstream sources several days ahead to mitigate the  $PM_{2.5}$  accumulations,  
344 rather than only taking actions when the pollution is already heavy. However, we must note that the two  
345 episodes we studied may not represent the general characteristics of heavy-pollution episodes, which requires  
346 a more systematic analysis in the future.

347 The current study has several limitations. We only quantify the  $PM_{2.5}$  transport at the outer boundary of the  
348 city, ignoring the inter-city transport of gaseous precursors that may be converted to secondary  $PM_{2.5}$  in the  
349 target city. Additionally, we cannot distinguish whether the  $PM_{2.5}$  inflows through the administrative boundary  
350 come from the neighbor city or upstream areas. Future studies may combine the flux calculation with the tracer  
351 or tagging methods to overcome these defects. Despite these limitations, the flux approach has indeed proved  
352 to be a powerful tool to visually assess the inter-city transport of pollutants.

353



## 354 **Acknowledgments**

355 We hereby express our gratitude to Yangjun Wang from Shanghai University, Jia Xing from Tsinghua  
356 University and Jiandong Wang from Max Planck Institute who helped us set up the modelling system and gave  
357 us useful suggestions.

358 This research has been supported by National Science Foundation of China (21625701 & 21521064). The  
359 simulations were completed on the “Explorer 100” cluster system of Tsinghua National Laboratory for  
360 Information Science and Technology.

361

## 362 **References**

363 An, J., Li, J., Zhang, W., Chen, Y., Qu, Y., and Xiang, W.: Simulation of transboundary transport fluxes of air  
364 pollutants among Beijing, Tianjin, and Hebei Province of China, *Acta Scientiae Circumstantiae*, 32, 2684-  
365 2692, 2012.

366 An, X., Zhu, T., Wang, Z., Li, C., and Wang, Y.: A modeling analysis of a heavy air pollution episode occurred  
367 in Beijing, *Atmospheric Chemistry and Physics*, 7, 3103-3114, 2007.

368 Berge, E., and Jakobsen, H. A.: A regional scale multi-layer model for the calculation of long-term transport  
369 and deposition of air pollution in Europe, *Tellus Series B-Chemical and Physical Meteorology*, 50, 205-  
370 223, 10.1034/j.1600-0889.1998.t01-2-00001.x, 1998.

371 BJEPB: Preliminary study of the atmospheric environment protection strategy in The 12th Five-year Plan,  
372 Beijing, China, 44-56, 2010.

373 BJEPB: Beijing Environmental Statement 2014, in,  
374 <http://www.bjepb.gov.cn/bjepb/resource/cms/2015/04/2015041609380279715.pdf>, 2015.

375 Cai, S., Wang, Y., Zhao, B., Wang, S., Chang, X., and Hao, J.: The impact of the "Air Pollution Prevention and  
376 Control Action Plan" on PM<sub>2.5</sub> concentrations in Jing-Jin-Ji region during 2012-2020, *The Science of  
377 the total environment*, 580, 197-209, 10.1016/j.scitotenv.2016.11.188, 2017.

378 Emery, C., Tai, E., and Yarwood, G.: Enhanced meteorological modeling and performance evaluation for two  
379 Texas episodes, Prepared for the Texas Natural Resource Conservation Commission, by ENVIRON  
380 International Corp, Novato, CA, 2001.

381 Fu, X., Wang, S., Zhao, B., Xing, J., Cheng, Z., Liu, H., and Hao, J.: Emission inventory of primary pollutants



- 382 and chemical speciation in 2010 for the Yangtze River Delta region, China, *Atmospheric Environment*,  
383 70, 39-50, 10.1016/j.atmosenv.2012.12.034, 2013.
- 384 Fu, X., Wang, S., Chang, X., Cai, S., Xing, J., and Hao, J.: Modeling analysis of secondary inorganic aerosols  
385 over China: pollution characteristics, and meteorological and dust impacts, *Scientific Reports*, 6,  
386 10.1038/srep35992, 2016.
- 387 Heald, C. L., Jacob, D. J., Park, R. J., Russell, L. M., Huebert, B. J., Seinfeld, J. H., Liao, H., and Weber, R.  
388 J.: A large organic aerosol source in the free troposphere missing from current models, *Geophysical*  
389 *Research Letters*, 32, 10.1029/2005gl023831, 2005.
- 390 Holton, J. R., and Hakim, G. J.: An introduction to dynamic meteorology, 5th ed., Elsevier, MA, USA, 532  
391 pp., 2012.
- 392 In, H.-J., Byun, D. W., Park, R. J., Moon, N.-K., Kim, S., and Zhong, S.: Impact of transboundary transport of  
393 carbonaceous aerosols on the regional air quality in the United States: A case study of the South American  
394 wildland fire of May 1998, *Journal of Geophysical Research-Atmospheres*, 112, 10.1029/2006jd007544,  
395 2007.
- 396 Itahashi, S., Uno, I., and Kim, S.: Source Contributions of Sulfate Aerosol over East Asia Estimated by  
397 CMAQ-DDM, *Environmental Science & Technology*, 46, 6733-6741, 10.1021/es300887w, 2012.
- 398 Jenner, S. L., and Abiodun, B. J.: The transport of atmospheric sulfur over Cape Town, *Atmospheric*  
399 *Environment*, 79, 248-260, 10.1016/j.atmosenv.2013.06.010, 2013.
- 400 Jia, Y., Rahn, K. A., He, K., Wen, T., and Wang, Y.: A novel technique for quantifying the regional component  
401 of urban aerosol solely from its sawtooth cycles, *Journal of Geophysical Research-Atmospheres*, 113,  
402 10.1029/2008jd010389, 2008.
- 403 Jiang, C., Wang, H., Zhao, T., and Che, H.: Modeling study of PM<sub>2.5</sub> pollutant transport across cities in China's  
404 Jing-Jin-Ji region during a severe haze episode in December 2013, *Atmospheric Chemistry and Physics*,  
405 5803-5814, 10.5194/acp-15-5803-2015, 2015.
- 406 Kwok, R. H. F., Baker, K. R., Napelenok, S. L., and Tonnesen, G. S.: Photochemical grid model  
407 implementation and application of VOC, NO<sub>x</sub>, and O<sub>3</sub> source apportionment, *Geoscientific Model*  
408 *Development*, 8, 99-114, 10.5194/gmd-8-99-2015, 2015.
- 409 Li, M., Zhang, Q., Kurokawa, J.-i., Woo, J.-H., He, K., Lu, Z., Ohara, T., Song, Y., Streets, D. G., Carmichael,  
410 G. R., Cheng, Y., Hong, C., Huo, H., Jiang, X., Kang, S., Liu, F., Su, H., and Zheng, B.: MIX: a mosaic





- 411 Asian anthropogenic emission inventory under the international collaboration framework of the MICS-  
412 Asia and HTAP, *Atmospheric Chemistry and Physics*, 17, 935-963, 10.5194/acp-17-935-2017, 2017.
- 413 Mu, Q., and Zhang, S.-q.: An evaluation of the economic loss due to the heavy haze during January 2013 in  
414 China, *China Environmental Science*, 33, 2087-2094, 2013.
- 415 Shi, C., Yao, Y., Zhang, P., and Qiu, M.: Transport Trajectory Classifying of PM<sub>10</sub> in Hefei, Plateau  
416 Meteorology, 27, 1383-1391, 2008.
- 417 Simon, H., and Bhawe, P. V.: Simulating the Degree of Oxidation in Atmospheric Organic Particles,  
418 *Environmental Science & Technology*, 46, 331-339, 10.1021/es202361w, 2012.
- 419 Stein, A. F., Draxler, R. R., Rolph, G. D., Stunder, B. J. B., Cohen, M. D., and Ngan, F.: NOAA'S HYSPLIT  
420 ATMOSPHERIC TRANSPORT AND DISPERSION MODELING SYSTEM, *Bulletin of the American*  
421 *Meteorological Society*, 96, 2059-2077, 10.1175/bams-d-14-00110.1, 2015.
- 422 Streets, D. G., Fu, J. S., Jang, C. J., Hao, J., He, K., Tang, X., Zhang, Y., Wang, Z., Li, Z., Zhang, Q., Wang,  
423 L., Wang, B., and Yu, C.: Air quality during the 2008 Beijing Olympic Games, *Atmospheric Environment*,  
424 41, 480-492, 10.1016/j.atmosenv.2006.08.046, 2007.
- 425 Wang, G., Zhang, R., Gomez, M. E., Yang, L., Zamora, M. L., Hu, M., Lin, Y., Peng, J., Guo, S., Meng, J., Li,  
426 J., Cheng, C., Hu, T., Ren, Y., Wang, Y., Gao, J., Cao, J., An, Z., Zhou, W., Li, G., Wang, J., Tian, P.,  
427 Marrero-Ortiz, W., Secret, J., Du, Z., Zheng, J., Shang, D., Zeng, L., Shao, M., Wang, W., Huang, Y.,  
428 Wang, Y., Zhu, Y., Li, Y., Hu, J., Pan, B., Cai, L., Cheng, Y., Ji, Y., Zhang, F., Rosenfeld, D., Liss, P. S.,  
429 Duce, R. A., Kolb, C. E., and Molina, M. J.: Persistent sulfate formation from London Fog to Chinese  
430 haze, *Proceedings of the National Academy of Sciences of the United States of America*, 113, 13630-  
431 13635, 10.1073/pnas.1616540113, 2016.
- 432 Wang, K., Zhang, Y., Jang, C., Phillips, S., and Wang, B.: Modeling intercontinental air pollution transport  
433 over the trans-Pacific region in 2001 using the Community Multiscale Air Quality modeling system,  
434 *Journal of Geophysical Research-Atmospheres*, 114, 10.1029/2008jd010807, 2009.
- 435 Wang, L., Wei, Z., Wei, W., Fu, J. S., Meng, C., and Ma, S.: Source apportionment of PM<sub>2.5</sub> in top polluted  
436 cities in Hebei, China using the CMAQ model, *Atmospheric Environment*, 122, 723-736,  
437 10.1016/j.atmosenv.2015.10.041, 2015.
- 438 Wang, W., Wang, Z., Wu, Q., Gbaguidi, A., Zhang, W., Yan, P., and Yang, T.: Variation of PM<sub>10</sub> Flux and  
439 Scenario Analysis before and after the Olympic Opening Ceremony in Beijing, *Climatic and*





- 440 Environmental Research, 15, 652-661, 2010.
- 441 Wang, Z., Li, J., Wang, Z., Yang, W., Tang, X., Ge, B., Yan, P., Zhu, L., Chen, X., Chen, H., Wand, W., Li, J.,  
442 Liu, B., Wang, X., Wand, W., Zhao, Y., Lu, N., and Su, D.: Modeling study of regional severe hazes over  
443 mid-eastern China in January 2013 and its implications on pollution prevention and control, Science  
444 China-Earth Sciences, 57, 3-13, 10.1007/s11430-013-4793-0, 2014.
- 445 Wu, P., Ding, Y., and Liu, Y.: Atmospheric circulation and dynamic mechanism for persistent haze events in  
446 the Beijing-Tianjin-Hebei region, Advances in Atmospheric Sciences, 34, 429-440, 10.1007/s00376-016-  
447 6158-z, 2017.
- 448 Zhang, Y., Ma, G., Yu, F., and Cao, D.: Health damage assessment due to PM<sub>2.5</sub> exposure during haze  
449 pollution events in Beijing-Tianjin-Hebei region in January 2013, National Medical Journal of China, 93,  
450 2707-2710, 2013.
- 451 Zhao, B., Xu, J., and Hao, J.: Impact of energy structure adjustment on air quality: a case study in Beijing,  
452 China, Frontiers of Environmental Science & Engineering in China, 5, 378-390, 10.1007/s11783-011-  
453 0357-8, 2011a.
- 454 Zhao, B., Wang, S., Wang, J., Fu, J. S., Liu, T., Xu, J., Fu, X., and Hao, J.: Impact of national NO<sub>x</sub> and SO<sub>2</sub>  
455 control policies on particulate matter pollution in China, Atmospheric Environment, 77, 453-463,  
456 10.1016/j.atmosenv.2013.05.012, 2013a.
- 457 Zhao, B., Wang, S. X., Liu, H., Xu, J. Y., Fu, K., Klimont, Z., Hao, J. M., He, K. B., Cofala, J., and Amann,  
458 M.: NO<sub>x</sub> emissions in China: historical trends and future perspectives, Atmospheric Chemistry and  
459 Physics, 13, 9869-9897, 10.5194/acp-13-9869-2013, 2013b.
- 460 Zhao, B., Wang, S. X., Xing, J., Fu, K., Fu, J. S., Jang, C., Zhu, Y., Dong, X. Y., Gao, Y., Wu, W. J., Wang, J.  
461 D., and Hao, J. M.: Assessing the nonlinear response of fine particles to precursor emissions: development  
462 and application of an extended response surface modeling technique v1.0, Geoscientific Model  
463 Development, 8, 115-128, 10.5194/gmd-8-115-2015, 2015.
- 464 Zhao, B., Wang, S., Donahue, N. M., Jathar, S. H., Huang, X., Wu, W., Hao, J., and Robinson, A. L.:  
465 Quantifying the effect of organic aerosol aging and intermediate-volatility emissions on regional-scale  
466 aerosol pollution in China, Scientific Reports, 6, 10.1038/srep28815, 2016.
- 467 Zhao, B., Wu, W., Wang, S., Xing, J., Chang, X., Liou, K.-N., Jiang, J. H., Jang, C., Fu, J. S., Zhu, Y., Wang,  
468 J., and Hao, J.: A modeling study of the nonlinear response of fine particles to air pollutant emissions in



469 the Beijing-Tianjin-Hebei region, Atmospheric Chemistry and Physics Discussions, 10.5194/acp-2017-  
470 428, 2017.

471 Zhao, P., Zhang, X., Xu, X., and Zhao, X.: Long-term visibility trends and characteristics in the region of  
472 Beijing, Tianjin, and Hebei, China, Atmospheric Research, 101, 711-718,  
473 10.1016/j.atmosres.2011.04.019, 2011b.

474 Zhao, Y., Wang, S., Duan, L., Lei, Y., Cao, P., and Hao, J.: Primary air pollutant emissions of coal-fired power  
475 plants in China: Current status and future prediction, Atmospheric Environment, 42, 8442-8452,  
476 10.1016/j.atmosenv.2008.08.021, 2008.

477



478 **Table 1 Summary of the emissions of major pollutants in Beijing, Tianjin and 11 prefecture-level cities**  
479 **in Hebei in 2012**

<b>Emissions (kt/year)</b>	NO <sub>x</sub>	SO <sub>2</sub>	PM <sub>2.5</sub>	PM <sub>10</sub>	BC	OC	NMVOCs	NH <sub>3</sub> <sup>a</sup>
<b>Beijing</b>	202	120	75	177	9	9	381	52
<b>Tianjin</b>	392	287	113	151	17	26	287	45
<b>Hebei</b>	1620	1079	875	1172	141	221	1346	628
Shijiazhuang	270	198	149	203	23	33	230	87
Chengde	84	45	37	49	6	10	56	34
Zhangjiakou	112	52	41	54	7	11	56	35
Qinhuangdao	71	39	30	40	5	8	51	22
Tangshan	266	145	100	135	15	24	181	68
Langfang	79	71	63	86	10	14	100	35
Baoding	158	123	118	155	20	33	202	89
Cangzhou	149	121	109	148	17	25	164	67
Hengshui	79	66	62	84	10	15	92	50
Xingtai	140	105	77	102	13	21	113	60
Handan	213	115	89	117	15	26	148	82

480

481 **Table 2 Comparison of the simulated and observed PM<sub>2.5</sub> concentrations at five sites.**

Indices	Mean OBS	Mean SIM*	NMB	NME	
Unit	$\mu\text{g}\cdot\text{m}^{-3}$	$\mu\text{g}\cdot\text{m}^{-3}$	%	%	
<b>January, 2012</b>	Beijing	86.0	65.2	-24.2	32.2
	Shijiazhuang	193.9	170.8	-11.9	45.3
	Xianghe	132.3	85.6	-35.3	44.5
	Xinglong	39.4	38.6	-2.0	42.7
	Yucheng	140.9	124.1	-11.9	31.2
<b>July, 2012</b>	Beijing	68.2	35.6	-47.8	49.5
	Shijiazhuang	70.3	79.8	+13.6	37.6
	Xianghe	61.3	47.2	-23.0	35.6
	Xinglong	48.9	24.6	-49.6	53.8
	Yucheng	77.3	55.2	-28.6	39.6

482 \*Average of the days only when observations are available.

483



484 **Table 3 The mean and maximum simulated PM<sub>2.5</sub> concentrations in Beijing for all days in January and**  
 485 **July and for the days that belong to particular transport pathways.**

Month	Pathway type	Days	Mean PM <sub>2.5</sub> conc in Beijing, $\mu\text{g}/\text{m}^3$	Max PM <sub>2.5</sub> conc in Beijing, $\mu\text{g}/\text{m}^3$
Jan	All days	31	65.2	270.7
	Southwest-Northeast	8	85.1	211.5
	Northwest-Southeast	22	58.6	270.7
	Unclassifiable day(s)	1	53.0	53.0
Jul	All days	31	35.0	94.4
	Southwest-Northeast	4	54.2	94.4
	Northwest-Southeast	5	15.4	30.9
	Southeast-Northwest	8	29.4	53.2
	SW-NE + SE-NW	8	47.4	71.0
	Unclassifiable day(s)	9	29.3	79.7

486



487 **Figure Captions**

488 **Figure 1.** The simulation domains used in this study (left) and the map of the Beijing-Tianjin-Hebei  
489 region (right). The highlighted cities are the target cities for flux calculation. The red circles show the  
490 sites with PM<sub>2.5</sub> observations. The two sites with green circles have observations of PM<sub>2.5</sub> chemical  
491 components in 2013.

492 **Figure 2.** Time series of the simulated and observed PM<sub>2.5</sub> concentrations in (a) Beijing, (b)  
493 Shijiazhuang, (c) Xianghe, (d) Xinglong, and (e) Yucheng.

494 **Figure 3.** An example of the vertical surface for flux calculation (a) before discretization, and (b) after  
495 discretization.

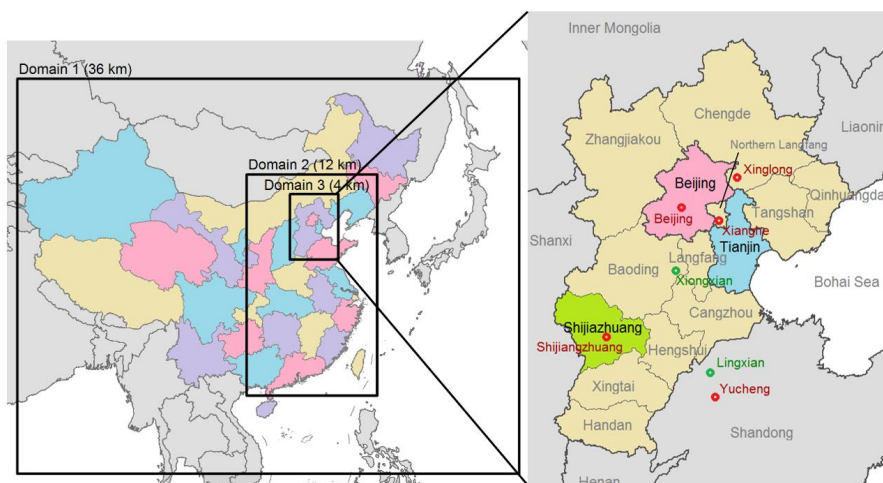
496 **Figure 4.** The inflow, outflow and net fluxes in January and July for (a) Beijing, (b) Tianjin, and (c)  
497 Shijiazhuang.

498 **Figure 5.** Vertical distribution of net fluxes in January (left) and July (right) for (a-b) Beijing, (c-d)  
499 Tianjin, and (e-f) Shijiazhuang

500 **Figure 6.** The transport fluxes through each boundary segment of the three target cities in January (left)  
501 and July (right). The size of the arrows represents the amount of the fluxes, while white and black arrows  
502 denote fluxes at the lower (layer 1-4 in the model, from the ground to about 400 m) and upper (layer 5-  
503 9 in the model, from about 400 m to about 1000 m) layers, respectively.

504 **Figure 7.** PM<sub>2.5</sub> fluxes during two heavy-pollution days in Beijing in January and July: (a) January  
505 17th, (b) January 18th, (c) July 18th and (d) July 20th.

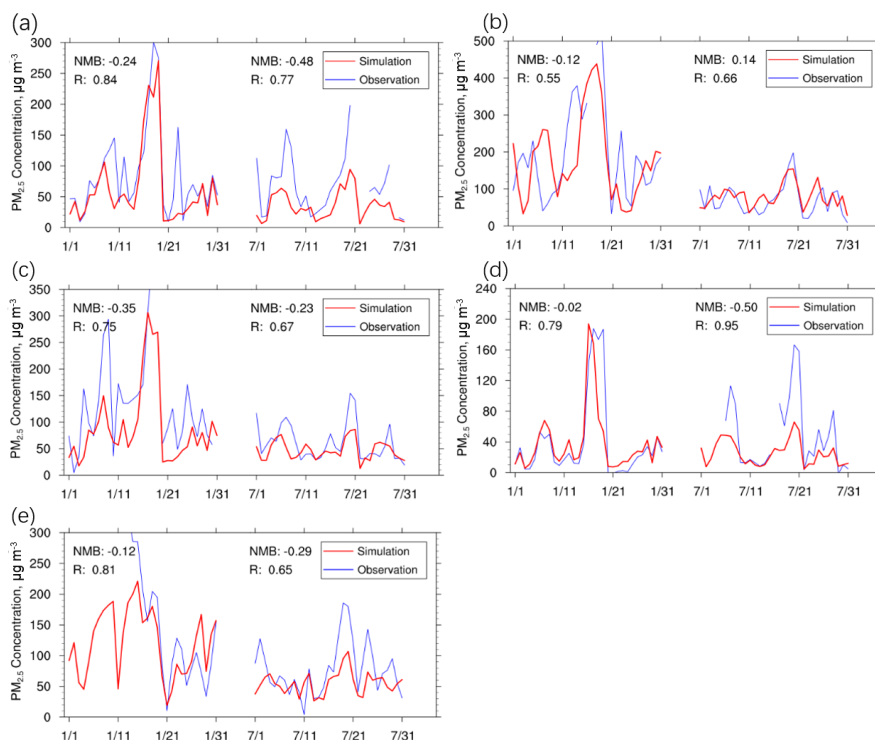
506



507

508 **Figure 1** The simulation domains used in this study (left) and the map of the Beijing-Tianjin-Hebei  
509 region (right). The highlighted cities are the target cities for flux calculation. The red circles show the  
510 sites with PM<sub>2.5</sub> observations. The two sites with green circles have observations of PM<sub>2.5</sub> chemical  
511 components in 2013.

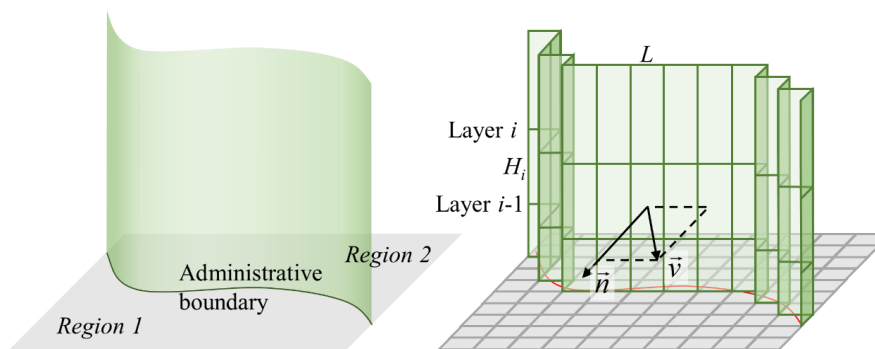
512



513

514 **Figure 2** Time series of the simulated and observed  $PM_{2.5}$  concentrations in (a) Beijing, (b) Shijiazhuang,  
 515 (c) Xianghe, (d) Xinglong, and (e) Yucheng

516

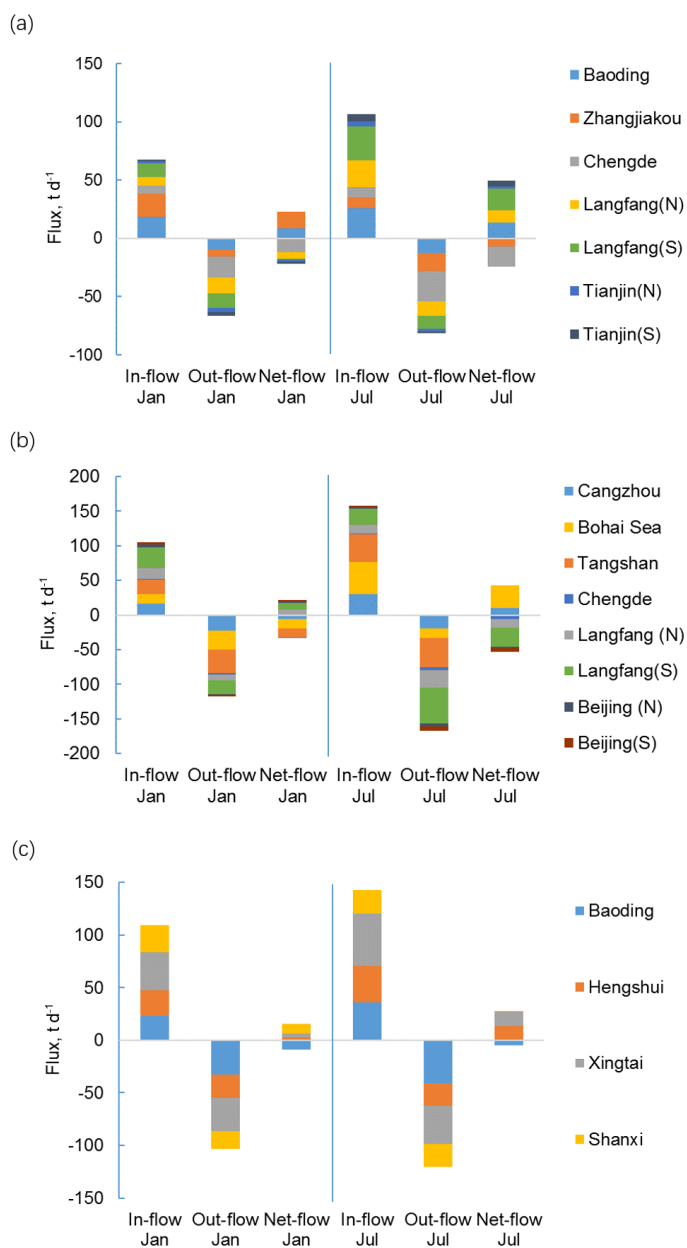


517

518 **Figure 3** An example of the vertical surface for flux calculation (a) before discretization, and (b) after  
 519 discretization.

520

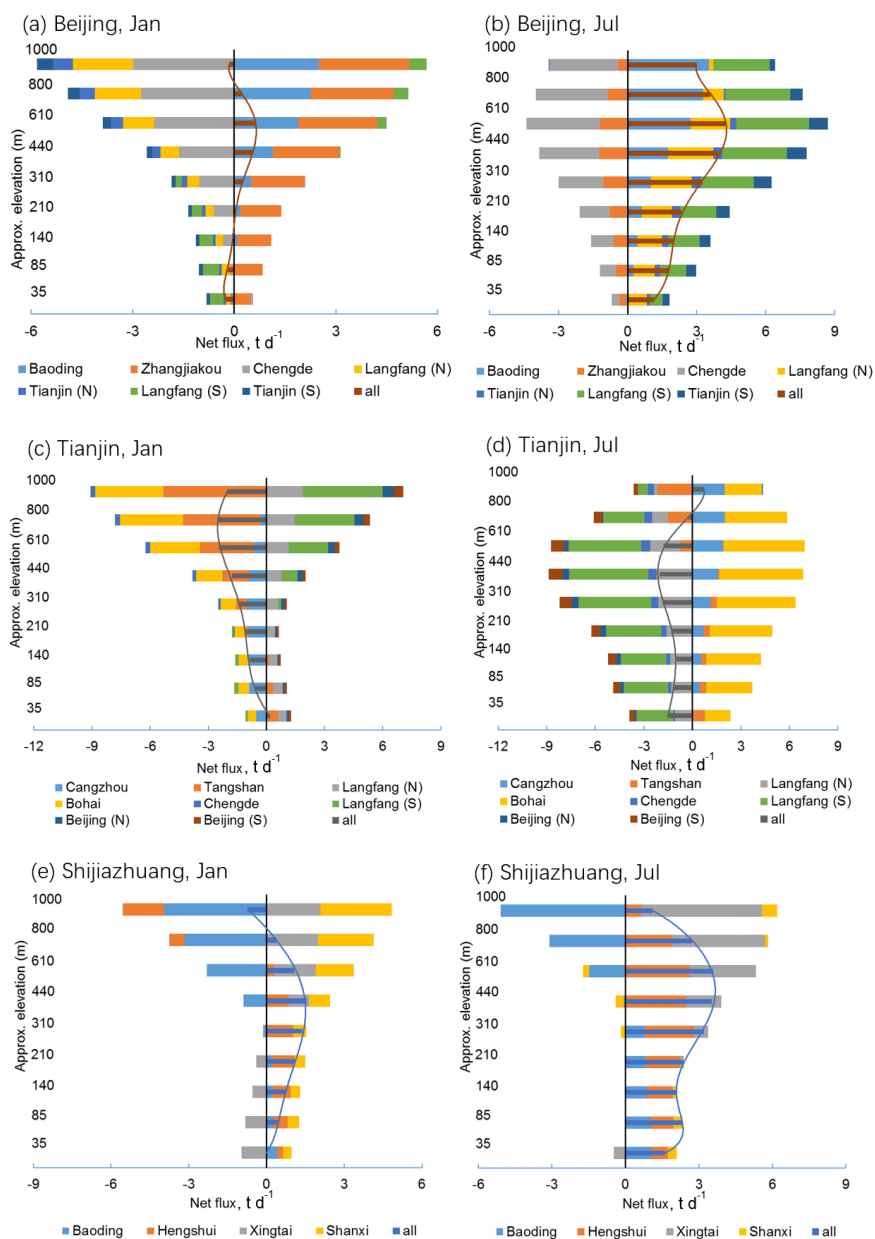




521

522 **Figure 4** The inflow, outflow and net fluxes in January and July for (a) Beijing, (b) Tianjin, and (c)  
523 **Shijiazhuang**

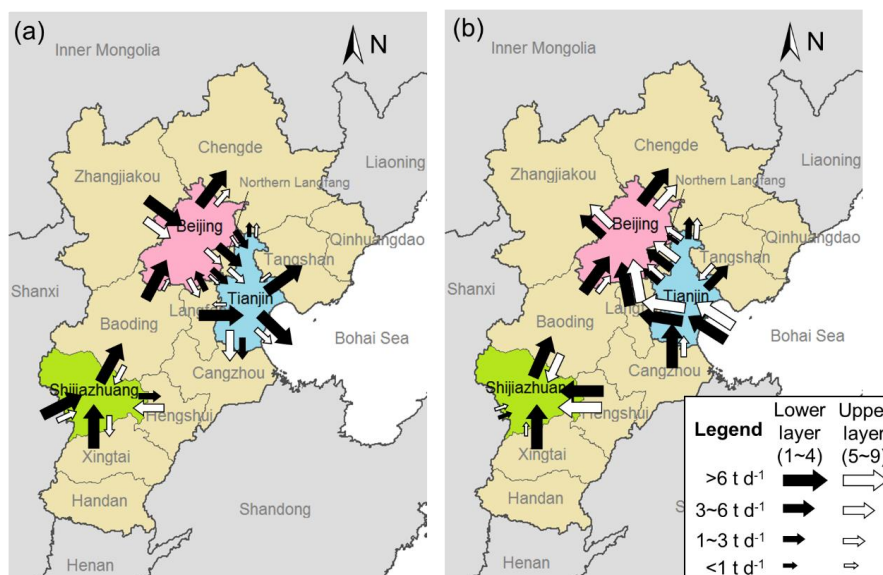
524



525

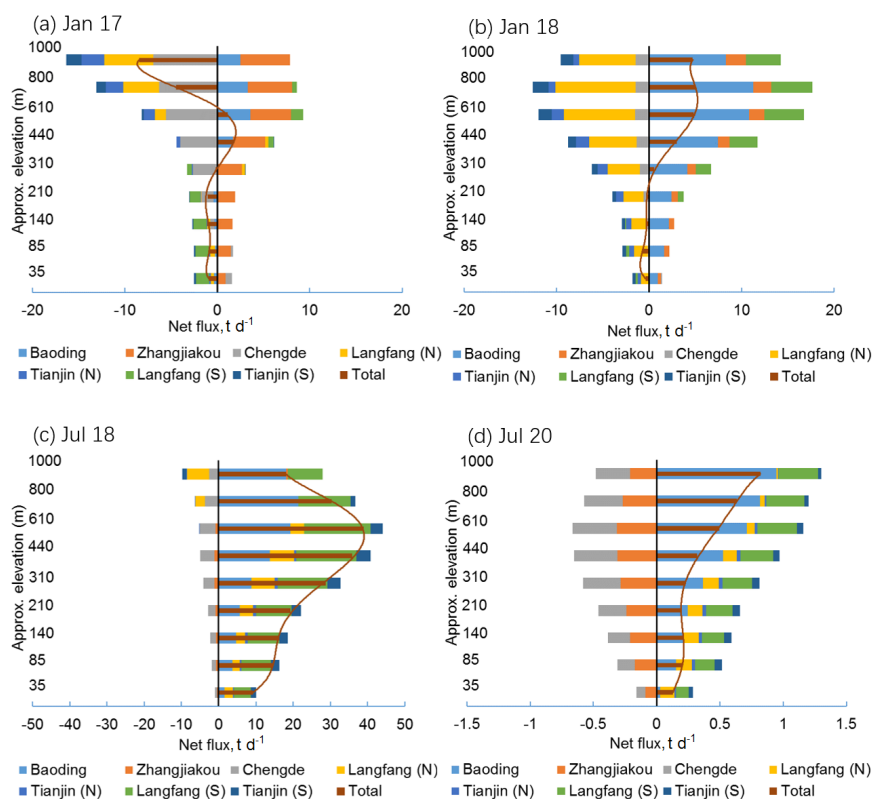
526 **Figure 5** Vertical distribution of net fluxes in January (left) and July (right) for (a-b) Beijing, (c-d)  
 527 Tianjin, and (e-f) Shijiazhuang

528



529

530 **Figure 6** The transport fluxes through each boundary segment of the three target cities in January (a)  
531 and July (b). The size of the arrows represents the amount of the fluxes, while white and black arrows  
532 denote fluxes at the lower (layer 1-4 in the model, from the ground to about 400 m) and upper (layer 5-  
533 9 in the model, from about 400 m to about 1000 m) layers, respectively.



534

535 **Figure 7** PM<sub>2.5</sub> fluxes during two heavy-pollution days in Beijing in January and July: (a) January 17th,  
536 (b) January 18th, (c) July 18th and (d) July 20th.

537